ACS APPLIED MATERIALS & INTERFACES

Research Article

Cite This: ACS Appl. Mater. Interfaces 2018, 10, 9225−9234

www.acsami.org

Surface Topography Hinders Bacterial Surface Motility

Yow-Ren Chang,[†] Eric R. Weeks,[‡] and William A. Ducker*[,†]

[†]Department of Chemical Engineering and Center for Soft Matter and Biological Physics, Virginia Tech, Blacksburg, Virginia 24061, United States

[‡]Department of Physics, Emory University, Atlanta, Georgia 30322, United States

Supporting Information

ABSTRACT: We demonstrate that the surface motility of the bacterium, *Pseudomonas aeruginosa*, is hindered by a crystalline hemispherical topography with wavelength in the range of 2−8 μm. The motility was determined by the analysis of time-lapse microscopy images of cells in a flowing growth medium maintained at 37 °C. The net displacement of bacteria over 5 min is much lower on surfaces containing 2−8 μm hemispheres than on flat topography, but displacement on the 1 μm hemispheres is not lower. That is, there is a threshold between 1 and 2 μm for response to the topography. Cells on the 4 μm hemispheres were more likely to travel parallel to the local crystal axis than in other directions. Cells on the 8 μm topography were less likely to travel across the crowns of the hemispheres and were also more likely to make 30°−50° turns than on flat surfaces. These results show that surface topography can act as a significant barrier to surface motility and may therefore hinder surface exploration by bacteria. Because surface exploration can be a part of the process whereby bacteria form colonies and seek nutrients, these results help to elucidate the mechanism by which surface topography hinders biofilm formation.

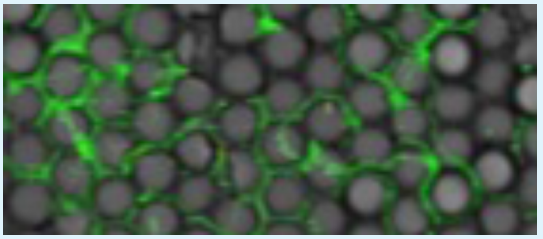

KEYWORDS: *biofilm, Pseudomonas aeruginosa, surface motility, time-lapse microscopy, surface topography*

1. INTRODUCTION

Bacterial biofilms are three-dimensional communities of bacteria encased in a self-secreted extracellular matrix.[1,2] Biofilms are formed when planktonic bacteria adhere to a surface, migrate, reproduce to form microcolonies, and produce an extracellular matrix.[3] Although bacteria often form biofilms in nature, they can be problematic in man-made systems. For example, biofilms can form inside industrial pipes[4] and on the exterior of ship hulls.[5,6] From a medical perspective, bacterial biofilms are sources of chronic and nosocomial infections,[7,8] causing patient suffering and mortality. It is estimated that hospital-acquired infections killed nearly 100 000 patients in the US in 2002 alone[9] and cost $17 billion to treat and manage.[10] Traditional antibiotic treatment of biofilms is difficult because the surrounding matrix provides a barrier to accessing the interior of the biofilm and is problematic because of the rise of antibiotic resistance.[11−13] Therefore, there is a growing need to develop methods to prevent bacterial biofilm formation on surfaces. Of particular interest to us are preventative methods that act locally at potential sites of infection, for example, on the surface of catheters. Local action is desirable to reduce the incidence of side effects, and preventative action is desirable to reduce the frequency of patient symptoms.

Several methods of preventing bacterial biofilm formation on surfaces are currently being researched. Notable examples include the use of oil-infused surfaces,[14] modifying the surface chemistry with antimicrobial peptides,[15] and mechanical methods to disrupt biofilms.[16] Recent studies have demonstrated that surface topography with micrometer-scale features also hinders bacterial adhesion and biofilm formation.[17−25] The Brennan group have produced a body of work showing that surface micro-topography mimicking that of shark skin inhibits the adhesion of several microorganisms.[26−29] Our laboratory recently reported that monolayers of closely packed, hexagonally arranged particles on a solid surface (colloidal crystals) hinder both the initial adhesion[30] and early biofilm formation[31] of the opportunistic human pathogen, *Pseudomonas aeruginosa*. Colloidal crystals formed from 1.5 μm diameter particles also reduced the biomass of early-stage *P. aeruginosa* biofilms by ∼80% compared to a flat surface.[31] Recent work shows a reduction of 99-99.9% on silica colloidal crystals and the independence of topographic and chemical treatments.[32]

These results suggest that surface topography could be a useful method for hindering biofilm formation. Yet the *mechanism* behind the action of surface micro-topography inhibiting biofilm growth is not well-understood. An understanding of the mechanism would aid in the design of new anti-biofilm surfaces. The development of biofilm is complex; many physical and environmental factors may impact biofilm formation.[33] Along the path to a biofilm, cells must first adhere to the surface, migrate (for surface motile cells), reproduce, and produce a matrix, and topography may affect any combination of these processes. Ideas on the mechanism have mainly focused on the effect of topography on adhesion. For example

Received: November 3, 2017
Accepted: February 22, 2018
Published: February 22, 2018

DOI: 10.1021/acsami.7b16715
ACS Appl. Mater. Interfaces 2018, 10, 9225−9234

Aizenberg's group has discussed the idea that the available *contact area* for adhesion is important,[34] and Brennan's group has considered the *number of contact points* for adhesion.[35] Our group has discussed the importance of *surface curvature* on adhesion.[30]

In this study, we focus on how curved surface micro-topography impacts the surface motility of single *P. aeruginosa* cells within 140 min of exposure to a solid. Previous work by Meel et al. examined the effect of rectilinear wall heights on the ability of *Neisseria gonorrhoeae* and *Myxococcus xanthus* to migrate over barriers.[36] Both these organisms and *P. aeruginosa* exhibit twitching motility, a type of surface motility facilitated by type IV pili.[37,38] It has been shown that twitching motility is required for biofilm formation[39] and can impact biofilm structure.[40] In this paper, we assess motility (active motion) using metrics such as the average distance travelled by the cell over a micropatterned surface. By using a flat surface as our control, our use of the word "motility" does not necessary imply cell "fitness" but includes the effects of the physical environment. This is the same as usage by Meel et al. By contrast, an alternative use of "motility" may exclusively refer to cell fitness that could be changed, for example, by genetic or regulatory changes.

In this work, we examine how motility is affected by the radius of curvature of the solid surface at constant surface chemistry. Because topography was the only factor, that is, chemistry was not a factor, we used polymer replicas of micro-topographic solids (Figure 1). To enable systematic variation of

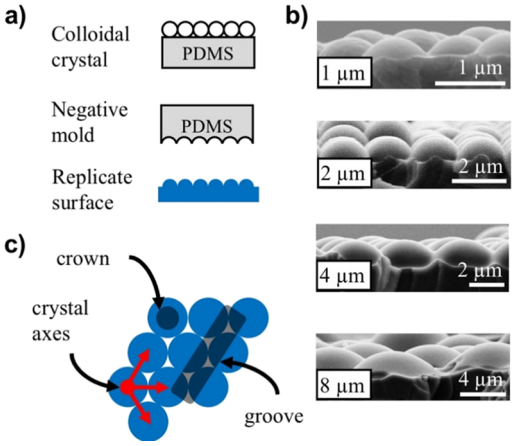

Figure 1. (a) Schematic of the fabrication of Norland Optical Adhesive (NOA) textured surfaces. A colloidal crystal made from SiO_2 particles is used as a topographical template. Using PDMS, a negative mold is created from the colloidal crystal, which is then used to create the samples of a single chemistry for the study of bacterial motility. (b) Cross-sectional scanning electron microscopy images of the sample surfaces show that the surface features are hemispherical. (c) Schematic describing the features of the textured surface.

the radius on a micrometer scale, we first fabricated monolayer colloidal crystals from monodisperse SiO_2 particles of diameter, d = 1, 2, 4, or 8 μm. For the uncurved (flat) control, we used the free surface of polydimethylsiloxane (PDMS). Negative molds were prepared, and then replicas were made such that all motility experiments utilized the same polymer, that is, the same chemistry (Figure 1a). The use of replicas meant that the topography is not spherical but rather a spherical cap (Figure 1a,b) that is approximately hemispherical. The micro-topography scatters visible light, so the cells are difficult to identify on the topography using transmission light microscopy. To enhance contrast for easier visualization, we utilized constitutively fluorescent bacteria and identified the cells from their fluorescent emission. The local topography was identified by phase-contrast imaging. As described in the Results section, tracking of the motion of these cells shows that the topography had a significant impact on motility.

Our interest is motion of the bacteria on the scale of the topography, that is, over displacements of approximately 1−8 μm. Typically, we find that bacteria traverse approximately 1 μm in 1 min, so we used a frame rate of 30 s to enable sampling that was faster than the average traverse time for the smallest feature. An example of a trajectory crossing our topography is shown in Figure 2. The intense light required for fluorescence

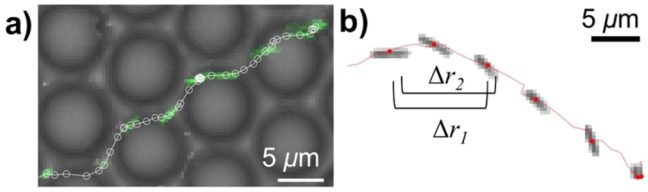

Figure 2. (a) Time-lapse imaging of bacterium (green) traversing an 8 μm textured surface. A time lapse of 30 s was chosen so that the bacterium could cross a large number of repeat features within the 120 min exposure limit that we set to minimize phototoxicity. The position of the bacterium at 30 s intervals is indicated by white circles, and every fifth image of the bacterium is shown (to limit overlap between images). (b) Time-lapse image of bacterium showing examples of the 5 min intervals that were used to obtain displacements.

imaging typically produces phototoxicity after about 100−400 frames, so there is a limited number of images that can be captured for each bacterium. We recorded movies that were 120 min long, which enabled sampling of motion on the length scale of the topography (1−8 μm) and for longer travel over multiple repeats of the topography. It is important to note that there is considerable complexity in surface motility and that some of these features are not examined here. Conrad et al. found that *P. aeruginosa* can crawl with the long axis of its body parallel to the surface or walk with the long axis perpendicular to the surface.[41] We observed that bacteria appear rodlike or circlelike in fluorescence and phase-contrast imaging, and following the work of Conrad et al.,[41] we attribute this effect to the different cross-section of the bacteria that is imaged. We do not distinguish between these orientations in our analysis. When *P. aeruginosa* is crawling, Jin et al. showed that the motion is characterized by a majority of slow movements with rare, rapid jumps, a movement termed as a slingshot.[42] We did not observe the motion during slingshots, as our imaging time point intervals (30 s) were far greater than the frame rates at which slingshot events were recorded (10 frames per s[42]).

2. MATERIALS AND METHODS

2.1. Fabrication of Colloidal Crystals and Topographical Replicas. The fabrication of topographical substrates used in this study is schematically shown in Figure 1. The templates for the curved features were stabilized colloidal-crystal monolayers that were fabricated, as described previously, with minor modifications.[43,44] In brief, colloidal crystals were fabricated using a rubbing method[45] in which monodisperse silica microspheres with diameters in the range of 1−8 μm (Fiber Optic Center, MA) were rubbed unidirectionally on a sheet of PDMS (Sylgard 184, Dow Corning). The PDMS sheets were prepared by mixing the base and curing agent in a 10:1 mass ratio,

DOI: 10.1021/acsami.7b16715
ACS Appl. Mater. Interfaces 2018, 10, 9225−9234

degassed, cast into 100 mm Petri dishes, and cured at 60 °C for 1 h. The crystallinity of the colloidal crystals was checked by observing the scattering pattern produced by the colloidal crystal from a 523 nm laser and also by inspection with optical microscopy. The 1 and 2 μm colloidal crystals were stabilized by formation of silica menscii from a sol−gel reaction of tetraethylorthosilicate (TEOS, Sigma-Aldrich).[43] The larger colloidal crystals were more difficult to stabilize using this method;[43] so instead, we spin-coated a prehydrolyzed TEOS solution onto the colloidal crystals following previously described methods.[44] To facilitate the release of the molded polymer from the crystal, an antiadhesion monolayer was attached to the colloidal crystal by activation with an O_2 plasma, followed by immersion in a 1% (v/v) solution of nonafluorohexyltricholorsilane (Gelest) in ethanol. After silane treatment, the samples were gently rinsed with ethanol and dried under N_2 gas streams. The negative mold was generated from PDMS. PDMS was mixed, degassed, and poured over the colloidal crystal samples and then cured overnight at 60 °C. An antiadhesion layer was also created on the stamp, as described above. Flat stamps were made from the PDMS cast into 100 mm Petri dishes and cured at 60 °C for 1 h. The free surface of the PDMS was used as the stamp.

The topographic samples were prepared from NOA 81 (Norland Products) molded by the PDMS stamp. NOA 81, when cured, is a stiff polymer with excellent optical transmittance in the visible light range and has been successfully used as a nontoxic culture substrate for the study of mammalian cells.[46] The cover glass (#1, 25 mm × 50 mm, Fisher Scientific) was cleaned using 10% sodium hydroxide, rinsed thoroughly with deionized water, dried using compressed N_2 gas, and then O_2 plasma-treated for 1 min at 100 W (Harrick Plasma). NOA was spin-coated onto the cover glass at 4000 rpm for 10 s (Laurell Technologies). Negative molds were placed onto the spin-coated slide, and air pockets were gently squeezed out. The NOA was initially cured using an Omnicure Series 1000 UV lamp (Excelitas Technologies) at 400 mW intensity from a distance of 6 in. for 2 min, and then the negative mold was removed. The NOA underwent a final cure in an ultraviolet/ozone cleaner (Bioforce Nanosciences) for 10 min. The molded topography was assembled into flow chambers[47] and sealed using PDMS.

The topographies of the NOA replicas were characterized using field emission scanning electron microscopy (FESEM, LEO 1550, Zeiss). For FESEM, the samples were fractured in liquid nitrogen and then sputter-coated with a 3 nm film of iridium using a Leica EM ACE600 sputter coater. For 1, 2, and 4 μm particles, the replicates were hemispheres of the same diameter as the particles (Figure 1b). For the 8 μm particles, the replicate had the appropriate width (8 μm) but was only about 2 μm high. The root-mean-square (rms) roughness of the flat surfaces and of the hemispherical particle features were measured using an Asylum Research Cypher ES atomic force microscope with Bruker ORC8-10 probes. For the textured surfaces, the topography was imaged on top of a hemispherical feature, and the image was first flattened with a second-order plane fit, and then the rms roughness was calculated. The rms roughness of all surfaces were very similar—in the range of 0.5−2 nm—and much smaller than the molded topographic features (~μm); so, we have distinct separation between size scales (see Figure 1b for dimensions of topography).

These final NOA samples will be referred to as textured samples as they are replicates of colloidal crystals and not actual colloidal crystals. It is important to note that the replica features are approximately hemispherical (Figure 1b). In contrast to actual colloidal crystals, there are no gaps between particles in which bacteria can dwell.

2.2. Bacterial Growth. The bacteria used in all experiments were *P. aeruginosa* PA01 that were genetically modified to constitutively express tdTomato fluorescent protein.[48] Frozen stocks of bacteria were stored at −80 °C in sterilized 30% glycerol. All solid and liquid media used to culture fluorescent bacteria were supplemented with 30 μg/mL gentamicin (Fisher Scientific). Bacteria were streaked onto tryptic soy agar plates and incubated at 37 °C overnight. A single colony was used to inoculate a 250 mL baffled flask with 50 mL of tryptic soy broth (30 g/L, TSB) capped with a foam stopper to allow air exchange. The flask was incubated at 37 °C and shaken at 300 rpm overnight (211DS, Labnet). Vigorous shaking and air exchange was necessary for good growth. The next day, a fresh culture was started in a 250 mL baffled flask with 50 mL of TSB and was inoculated with 50 μL of the overnight culture. This culture was grown to the early exponential phase (4 h), then diluted to OD_{600} = 0.01 in TSB, and used to inoculate the flow chamber.

2.3. Flow Cell Experiments. Our flow setup is similar to those described in the literature.[41,49] A home-built heater and microscope enclosure maintained the temperature at 37 °C throughout the experiment. The flow setup consisted of a media bottle containing TSB, a pump, a bubble trap, the flow chamber (1 mm × 4 mm cross section), and a waste container. Components were sterilized by autoclaving, and the flow chamber was separately sterilized using ethanol. Media was preflowed through the setup for at least 30 min prior to inoculation. Immediately before inoculation, flow was stopped, and the tubing was clamped to prevent backflow of the inoculum into the media bottle. Using a 26G syringe, 250 μL of the inoculum (diluted early exponential culture, see section 2.2) was injected into the flow chamber, and the chamber was inverted to allow bacteria to attach onto the surface. After 15 min, the flow chamber was returned to the topography-down orientation, and media flow was resumed at a rate of 4 mL/h. This flow washes away unattached cells and provides nutrients for the bacteria attached to the surfaces. Imaging then began immediately, that is, approximately 20 min after the inoculum was first injected into the flow chamber. Under these experimental conditions, the bacteria form an early biofilm if they are then cultured overnight.

2.4. Microscopy. Bacteria were imaged using an upright Zeiss Imager.M2 microscope equipped with a 63× oil immersion objective with a numerical aperture of 1.4 in brightfield and fluorescence. Owing to the short working distance of high numerical aperture lenses and the 1 mm deep fluid cell, the topographic sample was always situated between the image plane and the lens. Images were captured with a Zeiss Axiocam 506 mono camera with 5 × 5 binning (544 × 440 pixels). The binning reduces the pixel density of images and also decreases the exposure time required to image the bacteria. At these settings, bacteria are about 10 pixels in length and several pixels wide. The bacteria were imaged once every 30 s for 2 h. For flat, 1 μm, and 2 μm surfaces, two-dimensional movies were collected (bacteria were imaged at fixed stage heights). For 4 and 8 μm surfaces, *z*-stack movies were collected with 2 μm step intervals. The lamp intensity and exposure times were chosen to reduce phototoxicity. By comparing the motility of bacteria on flat glass surfaces that were imaged using only brightfield or fluorescence (see Figure S1), we found that our fluorescence imaging conditions did not impact the motility of the bacteria up to 1 h (120 exposures). Beyond 1 h, the speed of the bacteria imaged using fluorescence began to decrease. Therefore, we restricted our analysis of motility to the first hour of data since a bacterium was tracked. We also showed that the motility on flat samples was the same for wild-type and fluorescent bacteria (see Figure S2).

2.5. Bacteria Tracking and Data Analysis. Bacteria were automatically tracked using TrackMate,[50] an ImageJ plugin for particle tracking, which has been recently used to successfully track *P. aeruginosa*.[51] Trackmate identifies each cell and determines the centroid, and then the position of the centroid is tracked. The quality of the tracking was checked visually (see Figure 2) and by comparing displacement probability distributions for the bacteria on the flat sample that were obtained from TrackMate tracking and from manual tracking (see Figure S3). We did not find a significant difference between the manual and TrackMate tracking for this metric.

Starting about 20 min after the bacteria were first exposed to the solid, we recorded images at intervals of 30 s for a period of 120 min. The 30 s interval allows us to resolve movement through the topography, and 120 min of data were enough to track long paths and generate statistics. As described in the Introduction, we only included data for the first 60 min after a bacterium was first tracked. This was done so that data were only derived from bacteria that had 120 or fewer exposures to intense light.

In this work, we track all contributions to the movement of the centroid. Uniform growth of the cell does not affect the position of the centroid. Each cell division does affect the position of the centroid, but

DOI: 10.1021/acsami.7b16715
ACS Appl. Mater. Interfaces 2018, 10, 9225−9234

Table 1. Measured Parameters for Various Topographies[a]

particle size (μm)	microradius $d/2$ (μm)	roughness (nm) ± SE	displacement[d] r_{av} (μm) ± SE	decay length[e] (μm) ± SE	coverage per bacterium[f] (μm^2) ± SE	exponent[g] n ± 95% CI
flat	∞	1.5 ± 0.1	6.2 ± 0.3	16 ± 1.5	0.87 ± 0.19	1.51 ± 0.03
1	0.5	1.4 ± 0.2	5.0 ± 0.6	12 ± 0.5	0.81 ± 0.10	1.47 ± 0.04
2	1.0	1.1 ± 0.1	2.1 ± 0.3[b]	7 ± 1[b]	0.44 ± 0.09[b]	1.24 ± 0.01
4	2.0	1.9 ± 0.2	3.2 ± 0.2[b]	9 ± 0.5[b]	0.39 ± 0.03[b]	1.29 ± 0.04
8	<4[c]	0.7 ± 0.1	2.5 ± 0.3[b]	8 ± 0.8[b]	0.33 ± 0.01[b]	1.20 ± 0.04

[a]SE—standard error; CI—confidence interval for replicate experiments. [b]Indicates significant difference compared to the result on flat texture ($p < 0.05$). There was not a significant difference among the results for the 2, 4, and 8 μm surfaces or between the flat and 1 μm surface. [c]8 μm diameter and 2.4 μm height. [d]Average displacement in 5 min [e]Inverse of the slope of the $\log_{10}(P(\Delta r))$ data in Figure 5 for $\Delta r > 2$ μm. [f]Coverage in 100 min normalized by the average number of bacteria for images in Figure 3. [g]Fitted value of a in $\langle \Delta r^2 \rangle = a \cdot t^n$ for the data presented in Figure 6.

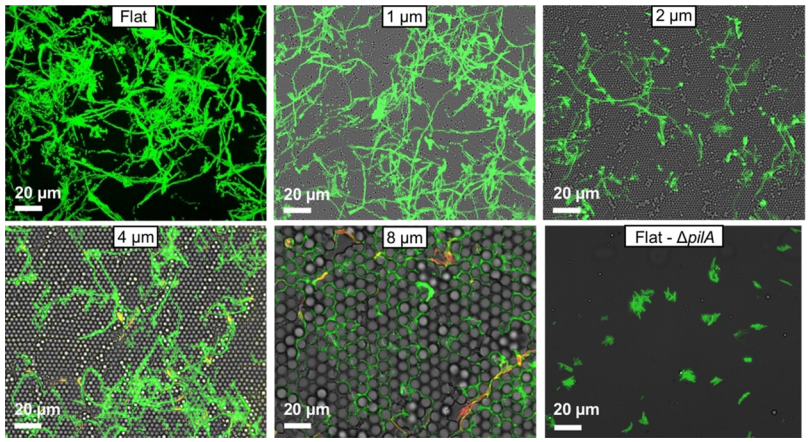

Figure 3. Intensity maximum in a 120 min time series of fluorescence images showing all areas of the surface visited by *P. aeruginosa* on a series of textured NOA solids. The texture is hemispheres made from replicas of colloidal crystals with diameter indicated (1−8 μm or flat). *P. aeruginosa* appears to explore a smaller fraction of the solid surface when there are features in the 2−8 μm range than for the flatter solids. The average number of bacteria on the images are 53, 51, 61, 46, and 105 for flat—8 μm and 56 for the Δ*pilA* on the flat for 60 min. The measured orientation order parameter for the topographies was ψ_6 = 0.68, 0.87, and 0.80 for 2, 4, and 8 μm, respectively.

the effect of division is small because (a) divisions are not that common (we typically observe ∼100 divisions out of ∼10 000 displacement events), and divisions sometimes increase and sometimes decrease the displacement, so there is a high degree of cancellation of the effects of division when calculating the average properties.

The surface coverage shown in Table 1 was determined by dividing an image into a 4 μm × 4 μm grid. If the centroid of a bacterium entered a grid, then that grid was considered to be covered. Note that this considers the projected area of the texture, not the actual contact area between the texture and the solution, which for perfect closely packed hemispheres would be 0.1 × 1 + 0.91 × 2 = 1.9 times greater than the projected area. The area available to the bacteria may be less on the molded topographical surfaces.

3. RESULTS

3.1. Bacteria Trajectories Depend on the Size Scale of the Surface Texture. The dimensions of *P. aeruginosa* on flat NOA samples measured by fluorescence microscopy were 2.90 ± 0.07 μm length and 1.21 ± 0.02 μm diameter, where ± refers to the standard error for 40 samples. Therefore, to examine how motility is affected by topography with dimensions similar to those of the bacteria, we examined motility on NOA samples textured with hemispheres with diameter in the range of 1−8 μm.

We captured 120 min time-lapse movies at 30 s intervals for each topography starting 20 min after the solid was first exposed to the bacteria. To obtain a visual impression of the trajectories of *P. aeruginosa* on various textured solids, Figure 3 shows the maximum intensity at each pixel for the 120 min time series. If a bacterium passes through a pixel, then a high intensity is recorded, and thus the maximum intensity image shows all locations covered by the bacteria. The depth of field of the objective is less than a few micrometers, so, on the 4 and 8 μm textured solids, at each time point, we rapidly captured a series of images at a series of different focus heights (a "*z*-stack") to sample the entire texture. Each height is given a different false color. Generally speaking, the bacteria do not appear to be moving at random, but often have a persistent overall direction. This effect is most obvious on the flat and 1 μm samples (Figure 3).

The images of the flat and 1 μm textures appear similar to each other, so we conclude that 1 μm hemispheres are too small to have much affect on bacterial motility. A number of qualitative features appear to be different on the 2, 4, and 8 μm textured surfaces compared to the flat and 1 μm solids, so there appears to be a threshold between 1 and 2 μm where motility is affected. If we were to examine even larger scale hemispheres, eventually we would expect that the cells might not be able to discriminate between a very large hemisphere (with a low curvature) and a flat surface. Evidently, 8 μm is not near such a limit as the behavior on the 8 μm topography was not similar to that on the flat topography. Because results on the flat and 1 μm samples are similar, we will sometimes refer to them together as the "low textures."

DOI: 10.1021/acsami.7b16715
ACS Appl. Mater. Interfaces 2018, 10, 9225−9234

A number of qualitative features appear to be different on the 2, 4 and 8 μm textured surfaces compared to that on the flat and 1 μm solids:

1 Images suggest that *P. aeruginosa* explores less of the solid surface when there are features in the 2−8 μm range than for 1 μm or flat surfaces: There is generally more color in the images of the low textures than in the high textures in Figure 3. This could be due to greater density of bacteria on the flatter solids or due to greater average speed on the texture. To reduce the effect of the density, we selected images for Figure 3 that had similar numbers of bacteria (see caption) so that it is clear that the effect is due to greater coverage per bacterium.
2 Trajectories on the 4 and 8 μm textures appear to be different: The bacteria tend to move in the valleys between hemispherical features and rarely over the crown of the hemispheres (see Figure 1c for an explanation of terms). As a result, some trajectories on these larger scale topographies are characterized by persistent straight runs in the direction of a crystal axis on the 4 μm texture, and some appear to move on a hexagonal grid on the 8 μm texture (Figure 4a,b).

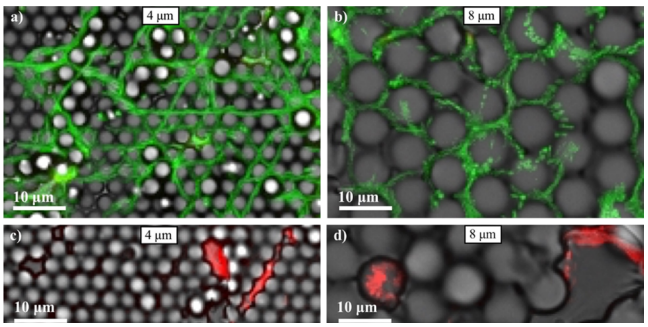

Figure 4. Enlarged sections of images showing the behavior of *P. aeruginosa* on the high textures. (a) On the 4 μm solid, there is greater propensity for straight-line motion and (b) on the 8 μm solid, there is a tendency to move approximately on a hexagonal grid. (c) Example of a bacterium moving along a line defect. (d) Example of a bacterium interacting with a hole defect.

3 Defects represent a different topography compared to the surrounding crystalline array of hemispheres: It is possible that such defects inhibit *P. aeruginosa* motility across a surface. Some bacteria do interact with surface defects such as holes (see Figure 4c,d) or a second layer of features. Note that because the hemispheres were templated from spheres, some holes in the tested topography are an entire diameter lower than the surrounding crowns (Figure 4d). Interactions with hole defects can be seen easily on the images because the bacteria that are on a low z-slice are colored red. Figure 4d, showing interaction with 8 μm features, indicates that some bacteria execute only small-scale excursions within a defect. However, we found that less than 10% of the bacteria in a movie interact with lower defects and that a majority of the cells interact with the hemispherical features. Therefore, our quantitative results are dominated by bacterial interactions with the crystalline array and not with topographical defects. In the following sections, we describe the results of our quantitative analysis of the time-series images.

3.2. Bacteria Have Greater Displacements on Flatter Textures. It would be interesting to know the velocity distribution of bacteria; on inspection of the videos, it is clear that the velocity is highly nonuniform over time; the bacteria dwell, change direction, and make sudden jumps, as has been described previously.[41] Therefore, we focus on the distance that the bacteria move over some period that is large enough so that some of this behavior is averaged out. Net distance moved also gives an indication of how much of a surface a bacterium is able to explore. We tracked each bacterium in a 158 μm × 196 μm field of view for 60 min and determined its net displacement over 5 min intervals. We measured approximately 5000 displacement events on each surface for one experiment and performed three replicate experiments.

We calculated the displacement (Δr) of a tracked bacterium over a time interval Δt at every tracked time point (t) from the x and y positions according to eq 1

$$\Delta r_t = \sqrt{(x_{t+\Delta t} - x_t)^2 + (y_{t+\Delta t} - y_t)^2} \quad (1)$$

We calculated Δr for Δt = 5 min for the first 60 min that a bacterium was tracked, that is, for the interval 0−5 min, 0.5−5.5 min, and so forth (see Figure 2b), with a bin size of 1 μm. We chose Δt = 5 min so that we could sample how far a bacterium has traversed on the scale of the topography. We also calculated Δr using different Δt values, and our conclusions do not change (see Figure S4). We did not include data for any bacterium that was tracked for less than 5 min

Our objective was to compare the average displacement of the bacteria on various topographies, but the distributions of displacements were non-normal, invalidating the use of conventional statistics for this comparison. To test the null hypothesis that the bacterial displacements were not different from each other on different surfaces, we utilized the central limit theorem and took averages of subsamples of the measurements. For each replicate experiment on each surface, we recorded the average of 100 randomly selected data points and performed this process 100 times. This yielded 100 subsampled averaged data points for each experiment. The distributions of these averaged points were indeed normal, which allowed us to perform routine statistical analyses. The average displacements of the 100 subsampled points for each replicate experiment for each experimental condition are shown in Table 1.

The average displacement was larger (5−6 μm) on the flat and 1 μm samples than on the higher topographies (2−2.5 μm). To test the null hypothesis that the mean displacements of bacteria on all surfaces were the same, we performed an analysis of variance (ANOVA). The p-value was 9×10^{-5}; hence, we reject the null hypothesis. Tukey's multiple comparison test showed that indeed bacterial displacements on flat and 1 μm surfaces were similar and that both were statistically different from displacements on higher textured surfaces, with the exception that the average displacement on the 1 μm surface was not statistically different from that on the 4 μm surface (p-value 0.07). (see Table 1, displacement data). There was not a significant difference among the results for the 2, 4, and 8 μm surfaces.

To examine the mechanism of motion on the surface, we explored the behavior of a Δ*pilA* mutant[52] on the flat surface. The Δ*pilA* mutant does not have a type IV pilus and therefore cannot exhibit twitching motility.[53] The average displacement of the Δ*pilA* mutant on the flat surface was 0.54 ± 0.01 μm,

DOI: 10.1021/acsami.7b16715
ACS Appl. Mater. Interfaces 2018, 10, 9225−9234

which is much less than that for the wild-type (6.2 ± 0.3 μm) and less than the length of the bacterium. The movement was restored in a complemented *pilA* strain (average displacement was 3.51 ± 0.13 μm, also see Figure S5 for maximum intensity images). This indicates that pilus-mediated motion is responsible for a large fraction of the movement that we observe in the wild-type.

Figure 5 shows the distribution of displacements. Displacement measurements were binned into 1 μm bins; the number

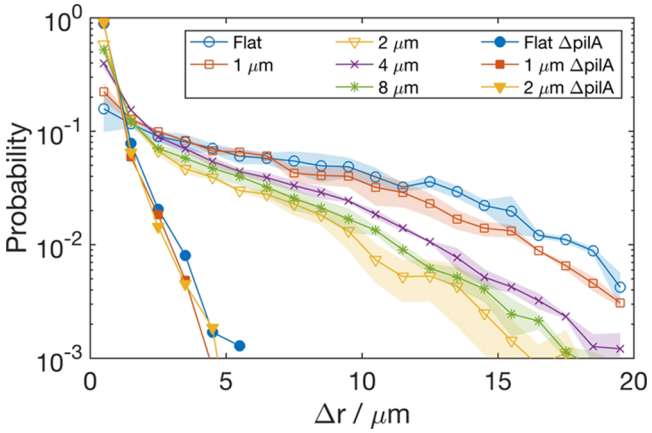

Figure 5. Probability/μm of displacement of *P. aeruginosa* over 5 min for a total of 60 min since tracked on a series of textured solids. The bin width was 1 μm, and the vertical scale is logarithmic. The symbols are the average, and the shaded region shows the standard error calculated from the probability at each Δr for the three replicates of the wild-type bacteria and the Δ*pilA* mutant. Note that the shaded regions for the Δ*pilA* mutant are too small to see. The lines are guides to the eye. There is a greater fraction of low-speeds for the 2−8 μm surfaces than for 1 μm or flat surfaces. Figure S4 shows representations of the same data, but the displacement was calculated for intervals of 1, 2, 5, and 10 min. These figures show that the probability distribution of bacteria on the flat and 1 μm spheres was also shifted to greater displacements for all these time intervals.

in each 1 μm interval was normalized by both the total number of Δr and by the bin size, to convert from counts to probability. We then averaged the probability at each interval for three replicate experiments to obtain the data in Figure 5.

The dispersion of behaviors of the wild-type bacteria suggests that it is also interesting to compare the range of displacements and not just the mean. Figure 5 shows, on a log scale, the measured probability distribution of distances traveled in 5 min, averaged across the three experiments. Figure 5 indicates a broad distribution of displacements on each texture. The displacement probability distribution of bacteria on a 1 μm textured surface was very similar to that of bacteria on a flat surface. This result suggests that bacterial motion was not strongly influenced by the 1 μm textured surface.

The displacement distributions of bacteria on higher textured surfaces (2−8 μm) were similar to each other but distinctly different from that of bacteria on the flat and 1 μm textured surfaces. In this group of higher textures, about 40−60% of the measured displacement events were less than 1 μm, whereas on the lower textures, only 15−25% of displacements were less than 1 μm. On the lower textures, about 15−20% of displacements were greater than 10 μm, but only about 5% had displacements this large on the lower surfaces. The distributions are approximately exponential (linear on the log scale of Figure 5) for displacements greater than 2 μm. The decay lengths for various topographies are given in Table 1. A Tukey multiple comparison test shows that the decay length for the flat surface is different from that of the 2, 4, and 8 μm topographies, but not significantly different from that of the 1 μm topography, as expected from Figure 5.

Some of the bacteria on the 4 or 8 μm textures are in low defects (colored red in Figures 3 and 4). In Figure 5, 2−10% of the data are from these low areas. Removal of these data does not significantly change Figure 5, but if we consider only the subset of data from the low areas, the long displacement (>10 μm) data are greatly reduced in probability.

To further quantify the motility of bacteria on the textured surfaces, we calculated the mean square displacement (MSD), $\langle \Delta r^2 \rangle$, of bacteria as a function of time time, t. For a random walk (diffusive behavior), $\langle \Delta r^2 \rangle = a \cdot t$, where a is a constant. We fitted our data from individual experiments to $\langle \Delta r^2 \rangle = a \cdot t^n$ for comparison (Figure 6), and the values of n are shown in Table

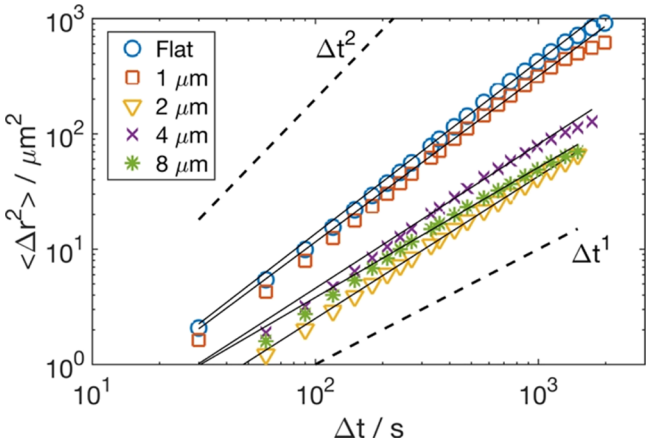

Figure 6. MSD of *P. aeruginosa* on flat and textured surfaces. The solid lines show regression fits to the data for each topography, and the dotted lines show the MSDs for a random walk ($\Delta t^{1.0}$) and ballistic motion ($\Delta t^{2.0}$) for comparison. *P. aeruginosa* was superdiffusive on all topographies, but n was greater on the smaller scale topography (n = 1.5, see Table 1) than on the larger scale topography (n = 1.2−1.3, see Table 1).

1. On all topographies, $n > 1$, indicating that bacterial motion was superdiffusive because of the tendency for bacteria to move in fairly straight lines over short time periods (see Figure 3). Again, data for the topographies fell into two categories. For the flatter textures, we found $n \approx 1.5$, which is very similar to the values previously reported for *P. aeruginosa* crawling motility on a flat surface.[41] For the larger scale topography (>2 μm), we found $n \approx 1.2$, that is, the motion is still superdiffusive but with a smaller exponent, which again indicates that the larger scale topography hindered motility. The 95% CIs (Table 1) do not overlap, showing that the difference in exponents between the large- and small-scale topographies is significant.

All textured surfaces were fabricated from the same material (NOA); therefore, we conclude that the surface topography hindered the surface motility of *P. aeruginosa*. Furthermore, there appears to be a threshold surface topographical feature size (between 1 and 2 μm) beyond which motility is hindered. This threshold size is similar to the bacterial dimensions (length ≈ 2.90 μm, diameter ≈ 1.21 μm).

Finally, to examine the visual impression from Figure 4 that bacteria visit more of the surface on the lower topographies, we also quantified the fraction of the surface that was visited by the

DOI: 10.1021/acsami.7b16715
ACS Appl. Mater. Interfaces 2018, 10, 9225−9234

set of bacteria in one field of view over 100 min by calculating the area coverage normalized by the average number of bacteria (Table 1). These results indicated that only about half as much of the surface was covered on the larger scale topography.

In the next section, we analyze why *P. aeruginosa* has shorter displacements on large-scale textures.

3.3. Direction of Motion of Bacteria is Influenced by the Underlying Topography. We first examined whether the *direction* of motion of a single bacterium was influenced by the surface texture. We determined the local crystal orientation (Figure 1c) by calculating ψ_6, the bond orientation order parameter,[54] and then calculated the angle, θ, between the crystal orientation and the bacterial velocity. Contributions from bacteria in the defective regions of the crystal were excluded by excluding from the analysis bacteria on regions where the local phase angle ψ_6 departed from the mean for the image by more than 10°. Figure 7a indicates that the averaged probability distribution of θ for three different experiments on highly ordered 4 μm textures all peaked at 0°. In other words, the bacteria have a tendency to move in the direction of the crystal axes. We then hypothesized that bacteria would move at a greater speed when moving in the direction of the crystal axes on the 4 μm texture. To test this hypothesis, we calculated the average displacement over 1 min as a function of θ (Figure 7b). We found that when bacteria do move in the direction of a crystal axis, they travel at a greater speed (Figure 7b). Although the speed is the greatest along the axis for the 4 μm texture, recall that the MSD is lower than on the flat and 1 μm textures.

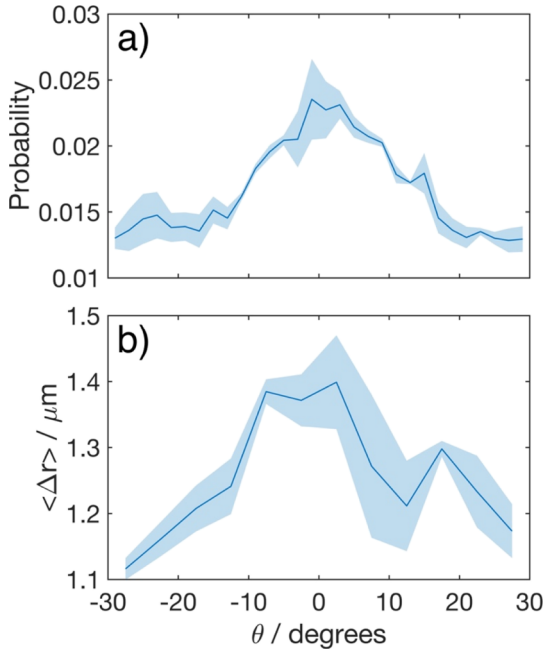

Figure 7. (a) Distribution of the angle of bacterial displacement *relative to the local lattice* on a 4 μm texture. Each displacement was measured over 1 min. (b) Mean displacements over 1 min. *P. aeruginosa* is more likely to travel along a crystal axis, and when it does so, it travels at a greater speed. Data shown are for 2 h of measurements for three independent samples. The line shows the average, and the shaded region is the standard error of three measurements. Both datasets in this figure must be symmetric about θ = 0° because of the symmetry in the topography. To test whether or not the bacteria do have a preferred direction and if they do travel at a greater speed, we performed statistical fits to determine (1) if there is a peak in both the datasets in this figure and (2) where the peak is located. For (a), the data was fit to a truncated normal distribution, and the fit was found to be significant (ANOVA, $p < 0.001$ compared no model), indicating that the distribution is not flat. The peak of the data is simply the mean of the fitted normal distribution, which is 0.5° ± 0.7°. For (b), the data was fitted to a parabola, and the fit was significant (ANOVA, $p < 0.001$ compared to no model), also indicating that there is a peak. The fitted peak was found to be 2° ± 2°.

In addition to a tendency to follow the crystal lattice, we also expected that bacteria would be more likely to change direction when they encounter a high obstacle. So, we examined the tendency of the bacteria to turn, that is, to vary the angular component of the velocity. The displacement was measured for each 2 min interval, and the angle between each two consecutive displacement vectors, $\Delta\theta$, was determined. To exclude small errors in tracking and small-scale oscillation of the bacterium, we only included cases where the bacterium displacement was 2 μm or more in consecutive intervals. Figure 8 shows the net change in the angle of motion, $\Delta\theta$. The inset in Figure 8 shows more detail for angles near 180°, that is, when the bacterium reverses direction. The figure suggests that bacteria are more likely to turn by more than 170° on the 2 and 8 μm topographies than on a flat surface, and a Tukey multiple comparison test confirms this ($p < 0.05$). Clearly, an increase in reversals decreases the net displacement, and these reversals are part of the reason for the smaller displacements on the larger scale topography.

The bacteria on the 8 μm texture have a greater probability of turning by 30−40° on 8 μm texture than on the flat (Tukey test, $p = 0.01$) (see Figure 8). Visual inspection of Figure 5 suggested that the bacteria on the 8 μm texture appear to move on the hexagonal lattice defined by the particles. If the bacteria followed a hexagonal lattice, we would expect to see a high probability of 60° turns. The increased probability at slightly lower angles indicates that the angular changes are affected by the lattice, but that it typically takes longer than 2 min to turn or that the bacteria cut corners, that is, the bacteria execute a gradual turn to negotiate the topography. In summary, the bacteria are more likely to make gradual turns from one lattice direction to another on the highest topography and more likely to make reversals on the 2 and 8 μm topography; both turns will reduce the distance travelled.

3.4. Colloidal Crystals Have a Similar Effect on *P. aeruginosa*. If topography is to be used to hinder the motility of bacteria in a practical application, such as a catheter coating, then the ease and cost of fabrication would be an important consideration. Colloidal crystals are much easier to prepare than polymer replicates: the colloidal crystal can be created in minutes; they can also be created on curved surfaces; and they are easy to stabilize.[55] Therefore, it is of interest to know whether the slowing of *P. aeruginosa* that we observed on replicates of colloidal crystals also occurs on colloidal crystals. Our experiments showed that the probability−displacement graph for the 1 μm colloidal crystal is very similar to that for the 1 μm template and likewise that the 2 μm colloidal crystal data are similar to those for the 2 μm template structure (see Figure 9). In common with the replicate samples, there is a distinct slowing of the bacteria on the 2 μm colloid crystal compared to that on the 1 μm colloidal crystal. This suggests that colloidal crystals may offer a simple, inexpensive coating to slow bacterial motion. It also suggests that the bottom half of the sphere on the colloidal crystal does not play a large role in affecting the motility for the 1−2 μm particle size range.

DOI: 10.1021/acsami.7b16715
ACS Appl. Mater. Interfaces 2018, 10, 9225−9234

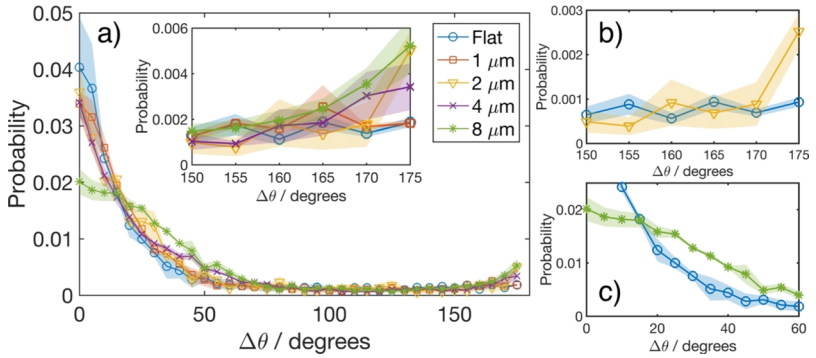

Figure 8. (a) Distribution of angular changes in the velocity over 2 min for *P. aeruginosa* for a series of texture surfaces. The total data set is 120 min long. (b) There is a greater probability of >170° turns on the 2 μm topography than on the flat. (c) On the 8 μm topography, there is a lesser probability of maintaining direction than on the other topographies and a greater probability of turning by 30°−40°.

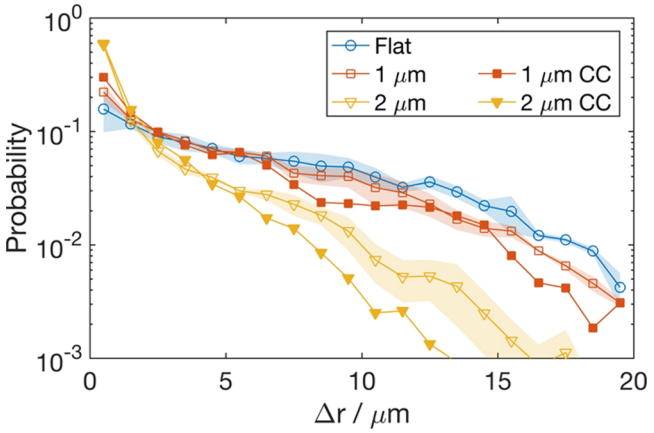

Figure 9. Comparison of probability/μm of displacement of *P. aeruginosa* for the colloidal crystal (filled-in markers) and template polymer (open markers). For the same radius, the colloidal crystal and template have similar probability distributions.

4. DISCUSSION

Previous studies by our lab demonstrated that colloidal crystals could inhibit the adhesion[30] and early biofilm formation of *P. aeruginosa*.[31] To form a biofilm, bacteria must first adhere to a surface, divide, organize into a microcolony, and secrete an extracellular matrix. We hypothesize that surface topography may hinder bacteria in a number of ways: during the initial adhesion, growth, communication, or motility of bacteria. In this work, we studied how the *surface motility* of *P. aeruginosa* was impacted by surface microtopography. We showed that, above a threshold feature size, about 1−2 μm, the displacement was significantly reduced and that a smaller amount of the surface was explored. One way for a bacterium to form microcolonies is to search over a surface to find other bacteria, so it is possible that this reduced motility hinders that ability of the bacteria to reach other bacteria and therefore to organize into microcolonies or larger structures. Previous work by Meel et al. found a similar threshold that affected the ability of *N. gonorrhoeae* and *M. xanthus* to migrate over barriers.[36]

A reduction in the average net displacement will also affect the net migration of bacteria. One route for infection of catheter patients is adsorption onto a catheter outside the body and migration into the body along the catheter. By reducing the speed of that migration, one may be able to reduce the incidence of catheter infections.

We are not yet in a position to determine how the topography affected motility, but here, we will briefly speculate on the effect. The textures for which we see reduced mobility are the 2, 4, and 8 μm textures with feature heights of 2, 4, and 2.4 μm, respectively. We find that the critical topographic height for obstruction is slightly larger than the diameter of the organism. *P. aeruginosa* (among other organisms) achieves surface motility using type IV pili[37,38] (∼5 μm in length[56]), which adhere to the solid in advance of a bacterium, and then the pilus is retracted and pulls the bacterium toward the point of adhesion.[53] Results of our Δ*pilA* mutant studies show that the absence of the pilus greatly reduces the displacement on three topographies (Figure 5) and therefore that the pili are agents of surface motility. We suggest that there are two requirements for the bacterium to advance across topography: (a) The end of pilus distant from the bacterium must be able to attach to a position on the solid from which it can apply a force. Attachment of the pilus requires a flight path for the pilus. (b) Once attached to the solid, the pilus must be able to apply a force to the pole of the bacterium with a component parallel to the direction of motion or be able to apply a torque to rotate the body into a favorable position for future motion. Now, considering the effect of topography, one can imagine that topography in front of the bacterium can block certain flight paths of the pili, and the topography under the bacterium can tilt the bacterial body such that the pilus is more or less likely to contact the solid in front of the pole. Convex surface topography, such as the hemispheres examined here, may tilt the body away from the attachment points for the pili. By contrast, in the grooves between hemispheres, there are features ahead of the pole that provide attachment points for the pili. When encountering a step, the pilus might not be able to reach over the step to strike an adhesion point that allows it to pull the bacterium forward. On a simplistic level, "retraction" of the pilus may bring the body up against a topographic feature such that the direction of force is being opposed by the riser of the solid. The force from the pilus acts on the pole of the bacterium at a point, which must be no higher than the maximum height of the bacterium. So when approaching a step, if the pilus is attached to the pole below the height of the step, the pilus may pull the bacterium toward the riser, and not over the step, thus hindering motion over the step. We intend to explore these mechanisms in future work.

DOI: 10.1021/acsami.7b16715
ACS Appl. Mater. Interfaces 2018, 10, 9225−9234

5. CONCLUSIONS

P. aeruginosa surface motility is hindered by micrometer-scale surface topographical features. Specifically, we found that the mean displacement of *P. aeruginosa* is significantly reduced by 2 μm diameter and larger hemispheres whereas smaller diameter features (1 μm) did not hinder motion. Furthermore, we found that, on 2 and 8 μm features, *P. aeruginosa* was more likely to reverse direction. On the 4 μm texture, the bacteria have greater displacement when traveling in approximately straight lines in the groove along the crystal axis than in other directions. On the 8 μm texture, the bacteria were more likely to turn to follow an approximately hexagonal lattice of groves between features. Overall, our data indicate that surface microtopography acts as a physical barrier that impedes the surface motility of *P. aeruginosa*. The reduced motility was also observed on monolayer coatings of particles. Hindering surface motility may be a route for hindering biofilm formation, which suggests a possible application of topographic coatings for medical devices.

■ ASSOCIATED CONTENT

Supporting Information

The Supporting Information is available free of charge on the ACS Publications website at DOI: 10.1021/acsami.7b16715.

Effect of fluorescence imaging on cell behavior compared to brightfield; comparison of the motion of the wild-type strain *P. aeruginosa* and a constitutively fluorescent strain; comparison of the displacement metric calculated from automated tracking to manual tracking; demonstration of the effect of different time intervals used to calculate displacement; and validation that the complemented pilA strain recovers the motion of the wild-type (PDF)

■ AUTHOR INFORMATION

Corresponding Author

*E-mail: wducker@vt.edu.

ORCID

Eric R. Weeks: 0000-0003-1503-3633

William A. Ducker: 0000-0002-8207-768X

Notes

The authors declare no competing financial interest.

■ ACKNOWLEDGMENTS

The authors thank the Institute for Critical Technology and Applied Science (ICTAS) at Virginia Tech and the Virginia Commonwealth Commercialization Fund (CRFC) (MF15-010-LS) for funding and support. We also thank the Nanoscale Characterization and Fabrication Laboratory (NCFL) at Virginia Tech for the use of their facilities. The authors also thank Dr. Joe Harrison at the University of Calgary for kindly providing all strains of *P. aeruginosa* used in these experiments and for useful suggestions and Trevor E. Randall for technical assistance. The work of E.R.W. was supported by the National Science Foundation (DMR-1609763). E.R.W. thanks W.·C. K. Poon for helpful discussions.

■ REFERENCES

(1) Hall-Stoodley, L.; Costerton, J. W.; Stoodley, P. Bacterial biofilms: from the natural environment to infectious diseases. *Nat. Rev. Microbiol.* **2004**, *2*, 95−108.

(2) Percival, S. L.; Malic, S.; Cruz, H.; Williams, D. W. Introduction to biofilms. *Biofilms and Veterinary Medicine*; Springer, 2011; pp 41−68.

(3) Monds, R. D.; O'Toole, G. A. The developmental model of microbial biofilms: ten years of a paradigm up for review. *Trends Microbiol.* **2009**, *17*, 73−87.

(4) Percival, S. L.; Walker, J. T. Potable water and biofilms: a review of the public health implications. *Biofouling* **1999**, *14*, 99−115.

(5) Townsin, R. L. The ship hull fouling penalty. *Biofouling* **2003**, *19*, 9−15.

(6) Schultz, M. P.; Bendick, J. A.; Holm, E. R.; Hertel, W. M. Economic impact of biofouling on a naval surface ship. *Biofouling* **2011**, *27*, 87−98.

(7) Costerton, J. W.; Stewart, P. S.; Greenberg, E. Bacterial biofilms: a common cause of persistent infections. *Science* **1999**, *284*, 1318−1322.

(8) Donlan, R. Biofilms and device-associated infections. *Emerging Infect. Dis.* **2001**, *7*, 277−281.

(9) Klevens, R. M.; Edwards, J. R.; Richards, C. L.; Horan, T. C.; Gaynes, R. P.; Pollock, D. A.; Cardo, D. M. Estimating Health Care-Associated Infections and Deaths in U.S. Hospitals, 2002. *Public Health Rep.* **2007**, *122*, 160−166.

(10) Hassan, M.; Tuckman, H. P.; Patrick, R. H.; Kountz, D. S.; Kohn, J. L. Cost of hospital-acquired infection. *Hosp. Top.* **2010**, *88*, 82−89.

(11) Mah, T.-F.; Pitts, B.; Pellock, B.; Walker, G. C.; Stewart, P. S.; O'Toole, G. A. A genetic basis for Pseudomonas aeruginosa biofilm antibiotic resistance. *Nature* **2003**, *426*, 306−310.

(12) Mah, T.-F. C.; O'Toole, G. A. Mechanisms of biofilm resistance to antimicrobial agents. *Trends Microbiol.* **2001**, *9*, 34−39.

(13) Stewart, P. S.; Costerton, J. W. Antibiotic resistance of bacteria in biofilms. *Lancet* **2001**, *358*, 135−138.

(14) Epstein, A. K.; Wong, T.-S.; Belisle, R. A.; Boggs, E. M.; Aizenberg, J. Liquid-infused structured surfaces with exceptional anti-biofouling performance. *Proc. Natl. Acad. Sci. U.S.A.* **2012**, *109*, 13182−13187.

(15) Iarikov, D. D.; Kargar, M.; Sahari, A.; Russel, L.; Gause, K. T.; Behkam, B.; Ducker, W. A. Antimicrobial Surfaces Using Covalently Bound Polyallylamine. *Biomacromolecules* **2014**, *15*, 169−176.

(16) Gu, H.; Lee, S. W.; Buffington, S. L.; Henderson, J. H.; Ren, D. On-Demand Removal of Bacterial Biofilms via Shape Memory Activation. *ACS Appl. Mater. Interfaces* **2016**, *8*, 21140−21144.

(17) Díaz, C.; Schilardi, P. L.; dos Santos Claro, P. C.; Salvarezza, R. C.; Lorenzo de Mele, M. A. F. Submicron Trenches Reduce the Pseudomonas fluorescens Colonization Rate on Solid Surfaces. *ACS Appl. Mater. Interfaces* **2009**, *1*, 136−143.

(18) Epstein, A. K.; Hong, D.; Kim, P.; Aizenberg, J. Biofilm attachment reduction on bioinspired, dynamic, micro-wrinkling surfaces. *New J. Phys.* **2013**, *15*, 095018.

(19) Ma, J.; Sun, Y.; Gleichauf, K.; Lou, J.; Li, Q. Nanostructure on taro leaves resists fouling by colloids and bacteria under submerged conditions. *Langmuir* **2011**, *27*, 10035−10040.

(20) Perni, S.; Prokopovich, P. Micropatterning with conical features can control bacterial adhesion on silicone. *Soft Matter* **2013**, *9*, 1844−1851.

(21) Xu, L.-C.; Siedlecki, C. A. Submicron-textured biomaterial surface reduces staphylococcal bacterial adhesion and biofilm formation. *Acta Biomater.* **2012**, *8*, 72−81.

(22) Lin, J.; Wen, G.; Peihong, X.; Hainan, G.; Ming, Z.; Chen, Z.; Yali, Z.; Dong, H. Quantitative assay for the colonization ability of heterogeneous bacteria on controlled nanopillar structures. *Nanotechnology* **2015**, *26*, 055702.

(23) Ling, G. C.; Low, M. H.; Erken, M.; Longford, S.; Nielsen, S.; Poole, A. J.; Steinberg, P.; McDougald, D.; Kjelleberg, S. Microfabricated polydimethyl siloxane (PDMS) surfaces regulate the development of marine microbial biofilm communities. *Biofouling* **2014**, *30*, 323−335.

(24) Ling, J. F., III; Graham, M. V.; Cady, N. C. Effect of topographically patterned poly (dimethylsiloxane) surfaces on

DOI: 10.1021/acsami.7b16715
ACS Appl. Mater. Interfaces 2018, 10, 9225−9234

pseudomonas aeruginosa adhesion and biofilm formation. *Nano LIFE* **2012**, *2*, 1242004.
(25) Bhattacharjee, A.; Khan, M.; Kleiman, M.; Hochbaum, A. I. Effects of Growth Surface Topography on Bacterial Signaling in Coculture Biofilms. *ACS Appl. Mater. Interfaces* **2017**, *9*, 18531−18539.
(26) Chung, K. K.; Schumacher, J. F.; Sampson, E. M.; Burne, R. A.; Antonelli, P. J.; Brennan, A. B. Impact of engineered surface microtopography on biofilm formation of Staphylococcus aureus. *Biointerphases* **2007**, *2*, 89−94.
(27) Reddy, S. T.; Chung, K. K.; McDaniel, C. J.; Darouiche, R. O.; Landman, J.; Brennan, A. B. Micropatterned surfaces for reducing the risk of catheter-associated urinary tract infection: an in vitro study on the effect of sharklet micropatterned surfaces to inhibit bacterial colonization and migration of uropathogenic Escherichia coli. *J. Endourol.* **2011**, *25*, 1547−1552.
(28) May, R. M.; Hoffman, M. G.; Sogo, M. J.; Parker, A. E.; O'Toole, G. A.; Brennan, A. B.; Reddy, S. T. Micro-patterned surfaces reduce bacterial colonization and biofilm formation in vitro: Potential for enhancing endotracheal tube designs. *Clin. Transl. Med.* **2014**, *3*, 8.
(29) Mann, E. E.; Manna, D.; Mettetal, M. R.; May, R. M.; Dannemiller, E. M.; Chung, K. K.; Brennan, A. B.; Reddy, S. T. Surface micropattern limits bacterial contamination. *Antimicrob. Resist. Infect. Contr.* **2014**, *3*, 28.
(30) Kargar, M.; Pruden, A.; Ducker, W. A. Preventing bacterial colonization using colloidal crystals. *J. Mater. Chem. B* **2014**, *2*, 5962−5971.
(31) Kargar, M.; Chang, Y.-R.; Hoseinabad, H. K.; Pruden, A.; Ducker, W. A. Colloidal Crystals Delay Formation of Early Stage Bacterial Biofilms. *ACS Biomater. Sci. Eng.* **2016**, *2*, 1039−1048.
(32) Mon, H.; Chang, Y. R.; Ritter, A. L.; Falkinham, J. O.; Ducker, W. A. Effects of Colloidal Crystals, Antibiotics, and Surface-bound antimicrobials on *Pseudomonas aeruginosa* Surface Density. *ACS Biomater. Sci. Eng.* **2018**, *4*, 257−265.
(33) Renner, L. D.; Weibel, D. B. Physicochemical regulation of biofilm formation. *MRS Bull.* **2011**, *36*, 347−355.
(34) Hochbaum, A. I.; Aizenberg, J. Bacteria pattern spontaneously on periodic nanostructure arrays. *Nano Lett.* **2010**, *10*, 3717−3721.
(35) Decker, J. T.; Kirschner, C. M.; Long, C. J.; Finlay, J. A.; Callow, M. E.; Callow, J. A.; Brennan, A. B. Engineered antifouling microtopographies: an energetic model that predicts cell attachment. *Langmuir* **2013**, *29*, 13023−13030.
(36) Meel, C.; Kouzel, N.; Oldewurtel, E. R.; Maier, B. Three-Dimensional Obstacles for Bacterial Surface Motility. *Small* **2012**, *8*, 530−534.
(37) Brill-Karniely, Y.; Jin, F.; Wong, G. C. L.; Frenkel, D.; Dobnikar, J. Emergence of complex behavior in pili-based motility in early stages of P. aeruginosa surface adaptation. *Sci. Rep.* **2017**, *7*, 45467.
(38) Mattick, J. S. Type IV pili and twitching motility. *Annu. Rev. Microbiol.* **2002**, *56*, 289−314.
(39) O'Toole, G. A.; Kolter, R. Flagellar and twitching motility are necessary for Pseudomonas aeruginosa biofilm development. *Mol. Microbiol.* **1998**, *30*, 295−304.
(40) Klausen, M.; Aaes-Jørgensen, A.; Molin, S.; Tolker-Nielsen, T. Involvement of bacterial migration in the development of complex multicellular structures in Pseudomonas aeruginosa biofilms. *Mol. Microbiol.* **2003**, *50*, 61−68.
(41) Conrad, J. C.; Gibiansky, M. L.; Jin, F.; Gordon, V. D.; Motto, D. A.; Mathewson, M. A.; Stopka, W. G.; Zelasko, D. C.; Shrout, J. D.; Wong, G. C. L. Flagella and Pili-Mediated Near-Surface Single-Cell Motility Mechanisms in P. aeruginosa. *Biophys. J.* **2011**, *100*, 1608−1616.
(42) Jin, F.; Conrad, J. C.; Gibiansky, M. L.; Wong, G. C. L. Bacteria use type-IV pili to slingshot on surfaces. *Proc. Natl. Acad. Sci. U.S.A.* **2011**, *108*, 12617−12622.
(43) Chang, Y.-R.; Taylor, S.; Duncan, S.; Mazilu, D. A.; Ritter, A. L.; Ducker, W. A. Fabrication of stabilized colloidal crystal monolayers. *Colloids Surf., A* **2017**, *514*, 185−191.
(44) Utech, S.; Bley, K.; Aizenberg, J.; Vogel, N. Tailoring re-entrant geometry in inverse colloidal monolayers to control surface wettability. *J. Mater. Chem. A* **2016**, *4*, 6853−6859.
(45) Park, C.; Lee, T.; Xia, Y.; Shin, T. J.; Myoung, J.; Jeong, U. Quick, Large-Area Assembly of a Single-Crystal Monolayer of Spherical Particles by Unidirectional Rubbing. *Adv. Mater.* **2014**, *26*, 4633−4638.
(46) Morgan, J. T.; Wood, J. A.; Shah, N. M.; Hughbanks, M. L.; Russell, P.; Barakat, A. I.; Murphy, C. J. Integration of basal topographic cues and apical shear stress in vascular endothelial cells. *Biomaterials* **2012**, *33*, 4126−4135.
(47) Tolker-Nielsen, T.; Sternberg, C. Growing and Analyzing Biofilms in Flow Chambers. *Current Protocols in Microbiology*; John Wiley & Sons, Inc., 2005.
(48) Shaner, N. C.; Steinbach, P. A.; Tsien, R. Y. A guide to choosing fluorescent proteins. *Nat. Methods* **2005**, *2*, 905−909.
(49) Nielsen, M. W.; Sternberg, C.; Molin, S.; Regenberg, B. Pseudomonas aeruginosa and Saccharomyces cerevisiae Biofilm in Flow Cells. *J. Visualized Exp.* **2011**, *47*, No. e2383.
(50) Tinevez, J.-Y.; Perry, N.; Schindelin, J.; Hoopes, G. M.; Reynolds, G. D.; Laplantine, E.; Bednarek, S. Y.; Shorte, S. L.; Eliceiri, K. W. TrackMate: An open and extensible platform for single-particle tracking. *Methods* **2017**, *115*, 80−90.
(51) Oliveira, N. M.; Foster, K. R.; Durham, W. M. Single-cell twitching chemotaxis in developing biofilms. *Proc. Natl. Acad. Sci. U.S.A.* **2016**, *113*, 6532−6537.
(52) Zhao, K.; Tseng, B. S.; Beckerman, B.; Jin, F.; Gibiansky, M. L.; Harrison, J. J.; Luijten, E.; Parsek, M. R.; Wong, G. C. L. Psl trails guide exploration and microcolony formation in Pseudomonas aeruginosa biofilms. *Nature* **2013**, *497*, 388−391.
(53) Burrows, L. L. Pseudomonas aeruginosa Twitching Motility: Type IV Pili in Action. *Annu. Rev. Microbiol.* **2012**, *66*, 493−520.
(54) Bernard, E. P.; Krauth, W. Two-Step Melting in Two Dimensions: First-Order Liquid-Hexatic Transition. *Phys. Rev. Lett.* **2011**, *107*, 155704.
(55) Chang, Y.-R.; Taylor, S.; Duncan, S.; Mazilu, D. A.; Ritter, A. L.; Ducker, W. A. Fabrication of stabilized colloidal crystal monolayers. *Colloid. Surf., A* **2017**, *514*, 185−191.
(56) Skerker, J. M.; Berg, H. C. Direct observation of extension and retraction of type IV pili. *Proc. Natl. Acad. Sci. U.S.A.* **2001**, *98*, 6901−6904.

DOI: 10.1021/acsami.7b16715
ACS Appl. Mater. Interfaces 2018, 10, 9225−9234